Assessment of High-Resolution Satellite-Based Rainfall Estimates over the Mediterranean during Heavy Precipitation Events

DIMITRIOS STAMPOULIS AND EMMANOUIL N. ANAGNOSTOU

Department of Civil and Environmental Engineering, University of Connecticut, Storrs, Connecticut

EFTHYMIOS I. NIKOLOPOULOS

Department of Land and Agroforest Environment, University of Padua, Padua, Italy

(Manuscript received 31 October 2012, in final form 19 March 2013)

ABSTRACT

Heavy precipitation events (HPE) can incur significant economic losses as well as losses of lives through catastrophic floods. Evidence of increasing heavy precipitation at continental and global scales clearly emphasizes the need to accurately quantify these phenomena. The current study focuses on the error analysis of two of the main quasi-global, high-resolution satellite products [Climate Prediction Center (CPC) morphing technique (CMORPH) and Precipitation Estimation from Remotely Sensed Imagery Using Artificial Neural Networks (PERSIANN)], using rainfall data derived from high-quality weather radar rainfall estimates as a reference. This analysis is based on seven major flood-inducing HPEs that developed over complex terrain areas in northern Italy (Fella and Sessia regions) and southern France (Cevennes–Vivarais region). The storm cases were categorized as convective or stratiform based on their characteristics, including rainfall intensity, duration, and area coverage. The results indicate that precipitation type has an effect on the algorithm's ability to capture rainfall effectively. Convective storm cases exhibited greater rain rate retrieval errors, while low rain rates in stratiform-type systems are not well captured by the satellite algorithms investigated in this study, thus leading to greater missed rainfall volumes. Overall, CMORPH exhibited better error statistics than PERSIANN for the HPEs of this study. Similarities are also shown in the two satellite products' error characteristics for the HPEs that occurred in the same geographical area.

1. Introduction

Heavy precipitation events (HPEs) are the main cause of catastrophic floods in complex terrain basins. HPEs are characterized by varying spatiotemporal characteristics: short-duration, heavy rain rates from convective storms or persistent moderate-intensity rainfall rates from stationary systems (Gaume et al. 2009; Ducrocq et al. 2008). Depending on the severity of the event and storm duration, floods caused by such events can be categorized as flash floods, which constitute one of the top-ranked natural disasters. The timely and reliable quantitative estimation of HPEs represents one of the most serious challenges to hydrometeorological research. Furthermore, there is evidence of increasing heavy precipitation at continental (Groisman et al. 2004) and global scales (Groisman et al. 2005), which emphasizes the need for accurate quantification of these storm events and will in turn provide more reliable data for flood modeling.

Up until recently, rain gauges had been undoubtedly the primary source of precipitation data. Although they have an undisputed advantage of directly measuring precipitation, they are severely plagued by their poor spatial resolution. Providing only point measurements, rain gauge distribution over land is highly uneven, while over mountainous basins the gauge coverage is very limited. Even the few relatively dense rain gauge networks over some continental areas (parts of the United States and Europe) are unable to depict the intensity and spatial extent of heavy precipitation (Scofield and Kuligowski 2003). Moreover, other sources of uncertainty (e.g., wind effects) can significantly impact the reliability of the rain gauge measurements.

The advent of weather radar technology and the establishment of national networks have partly addressed

Corresponding author address: Prof. Emmanouil Anagnostou, Civil and Environmental Engineering, University of Connecticut, 261 Glenbrook Rd., Unit 3037, Storrs, CT 06269.
E-mail: manos@engr.uconn.edu

DOI: 10.1175/JHM-D-12-0167.1

the gauge sampling issue. More spatially representative estimates of precipitation became available, which are, however, subject to various limitations. The conversion of the radar-measured reflectivity to rainfall rates is characterized by significant variability due to variations in the rainfall drop size distribution, surface effects, mixed-phase precipitation, and ground returns. Other issues include rain-path attenuation, beam blockage, beam filling, and beam overshoot effects (Gruber and Levizzani 2006; Krajewski and Smith 2002). Finally, as the distance from the radar increases, its efficiency to detect precipitation decreases, especially over mountainous terrain. Even for the most advanced national weather radar networks, the observational gaps over mountainous areas can be quite significant (Maddox et al. 2002).

As stated above, although radar-derived rainfall estimates are in many cases quite reliable, their coverage is still very limited relative to satellite observations (e.g., mountainous areas, developing regions like Africa, and parts of Asia), and this renders them less desirable for global hydrological applications. Also, deploying and maintaining a fully functional radar network is a very costly task, and in certain places of the world, this is not practical. Moreover, depending on the topography, there are regions where radar networks may not be deployed, such as high-elevation areas or areas with complex terrain in general. The only way to measure rainfall over these regions is through remote sensing from space. Finally, satellite techniques are constantly improving and are very promising with regards to detecting rainfall under different conditions (i.e., precipitation type). Therefore, a satisfactory way to compensate for some of the limitations that rain gauges and radars entail is by applying satellite remote sensing that provides nearly global coverage. These advantages have led to the existence of a significant number of satellite-based rainfall products that meet various hydrometeorological needs (Michaelides et al. 2009).

Satellite-based estimates of precipitation can be derived from various sensors. Depending on the type of observation, the retrieval methodologies are based on visible (VIS) or infrared (IR) techniques, active or passive microwave (MW) techniques, and multisensor techniques. Both approaches (VIS/IR and MW) are associated with errors and uncertainties. Arguably, the relationship between satellite-measured radiances and surface rainfall rate is less robust than that between radar reflectivity and rainfall (Scofield and Kuligowski 2003). More specifically, the relationship between cloud properties inferred from VIS/IR and surface precipitation is indirect; therefore, their link is weak (Anagnostou et al. 2010; Sapiano and Arkin 2009; Adler et al. 2000). Conversely, MW instruments provide rainfall estimates with greater accuracy, since their observations are related to the hydrometeor content present within the atmospheric column, but because of their low observational frequency and large sensor field of view areas, they suffer from larger sampling errors, and this is a limiting factor when dealing with short-term rainfall estimates (Kidd et al. 2003). One example of satellite algorithms that use exclusively passive microwave rain estimates is the Climate Prediction Center (CPC) morphing technique (CMORPH), while examples of satellite rainfall products that use both MW and IR are the Precipitation Estimation from Remotely Sensed Imagery Using Artificial Neural Networks (PERSIANN) and the National Aeronautics and Space Administration's (NASA) Tropical Rainfall Measuring Mission (TRMM) Multisatellite Precipitation Analysis (TMPA) (Huffman et al. 2007).

Previous research has shown that the accuracy of satellite rainfall data is subject to precipitation type (convective or stratiform), topography of the region (e.g., complex terrain), and climatological factors (Tang and Hossain 2012; Stampoulis and Anagnostou 2012; Scheel et al. 2010; Dinku et al. 2008; Jiang et al. 2008; Artan et al. 2007; Schumacher and Houze 2003; Scofield and Kuligowski 2003; Steiner and Smith 1998). Furthermore, since stratiform and convective precipitation may occur in adjacent regions of a convective system, this poses considerable problems when retrieving rainfall intensity from satellites (Levizzani 1999). Accurate quantification of precipitation occurring during short-term storm events (of both convective and stratiform origin) is a very difficult problem that satellite rainfall retrievals are continuing to address. There have only been a few studies assessing the error of satellite algorithms for heavy precipitation and mountainous areas. Turk et al. (2006) analyzed rainfall accumulations derived from CMORPH and four other satellite-based precipitation techniques during the landfall of Hurricane Wilma over the Yucatan Peninsula in Mexico and compared them to the rainfall measured by rain gauges. Time series of the maximum accumulated precipitation both over ocean and land clearly showed that CMORPH underestimated rainfall in both cases, especially over ocean.

In another study, Demaria et al. (2011) examined the ability of three satellite products (TRMM, CMORPH, and PERSIANN) to represent the spatial characteristics of mesoscale convective systems over the La Plata River basin in southeastern South America. The evaluation was performed against observed precipitation (obtained from an extended rain gauge network). CMORPH exhibited overestimation against ground observations for rainfall accumulation exceeding $30\,\mathrm{mm\,day^{-1}}$, while PERSIANN estimates were lower than observations. However, the spatial extent of mesoscale convective

systems was found to be overestimated by PERSIANN, which exhibited systematically larger storm areas than observations. Moreover, both CMORPH and PERSIANN successfully captured the maximum rainfall of the storm events, while high rainfall rates were underestimated at all times.

AghaKouchak et al. (2011) also evaluated satellite-derived precipitation products [CMORPH, PERSIANN, near-real-time TMPA (TMPA-RT), and TMPA version 6 (TMPA-V6)] with respect to their performance in capturing precipitation extremes. Weather Surveillance Radar-1988 Doppler (WSR-88D) stage IV (gauge adjusted) radar-rainfall data were used as reference in their analysis. They found that CMORPH, PERSIANN, and TMPA-RT overestimated precipitation, particularly in the warm season, and this overestimation increased significantly for higher thresholds of reference data. Furthermore, among the different satellite products, PERSIANN exhibited the lowest bias regardless of the reference threshold, while TMPA-RT estimates showed the highest bias over all thresholds. Moreover, CMORPH and PERSIANN were found to perform better in detecting precipitation areas, but as the threshold increased, their skill to detect rainfall volumes decreased. Overall, CMORPH and PERSIANN were found to miss the least amount of rainfall volume and as the rainfall thresholds increased, so did the volume of missed rainfall. Lastly, CMORPH and PERSIANN consistently exhibited higher false alarm ratios than TMPA-RT.

Prat and Barros (2010) conducted a study in which rain gauge observations were used as reference to assess precipitation estimates from the Precipitation Radar (PR 2A25) on board the TRMM satellite for a period of one year that includes Tropical Storm Fay. Overall, they found that the bias for TRMM PR 2A25 is approximately 27% underestimation for the 1-yr study period, while in the case of the tropical storm, a much greater bias was observed (-59%). In both cases, the mismatch corresponded to low and moderate rainfall regimes, with most of the misses being in the light rainfall range. Finally, in a case study, Salio et al. (2007) validated CMORPH data over the central region of Argentina for a period of successive convective systems that generated strong rainfall rates and extensive floods. Daily accumulated rainfall observed by gauges was used to validate CMORPH rainfall estimates. They showed that CMORPH represented well the region associated with the flooded area, and in general, extreme values were well detected.

Arguably, current satellite rainfall estimates are associated with significant uncertainty over land. Therefore, information on satellite rainfall products' performance for different precipitation types (stratiform versus convective), over different climatic regions, and for various levels of terrain complexity is essential for understanding and improving the deficiencies of current retrieval algorithms; this information can further contribute to the accurate characterization of satellite rainfall error structure (e.g., the dependence on rainfall magnitude, temporal variability, etc.) and can therefore lead to more reliable precipitation estimates at global scale. Along these lines, the current study is focused on the detailed error analysis of two of the main quasi-global, high-resolution satellite products (CMORPH and PERSIANN) for seven major HPEs that occurred over mountainous areas in northern Italy (Fella and Sessia regions) and southern France (Cevennes–Vivarais region). The study regions are prone to hydrologic extremes because of the terrain's high complexity, which in turn acts as the driver of flood-inducing rain events. The analysis is performed based on reference rainfall data derived from rain gauge–calibrated weather radar rainfall estimates. All HPEs were reported as flood-inducing storms, some of which are characterized by very high return periods (>100 yr). The aim of this study is to provide quantitative information about the error structure of CMORPH and PERSIANN products during these major precipitation events. As a result, this work should contribute toward understanding the error characteristics, which can provide feedback to algorithm developers and those involved in error modeling and can therefore lead to improved accuracy estimates of HPEs. Ultimately, results from this study should help hydrologists understand the usefulness of satellite-derived rainfall estimates for flood modeling. In the next section, we will discuss the study regions and storm cases used for the satellite error analysis. In section 3 we discuss the data and the error methodology, while in section 4 we present the results.

2. Study regions and storm cases

We selected seven major storm events over three different mountainous regions (Fella, Sesia, and Cevennes–Vivarais) in the western Mediterranean. The study regions are shown in Fig. 1, and the selected storms are summarized in Table 1. Below, we discuss the characteristics of the study areas and storm cases.

Fella, located in northeastern Italy, specifically the Friuli–Venezia Giulia region, includes a portion of the central chain of eastern Alps (Borga et al. 2007); its mean elevation is approximately 1200 m MSL and it borders to the north with Austria, to the east with Slovenia, and to the west with Veneto. Overall, the mean annual precipitation ranges from 1200 to 3300 mm, with spatial distribution controlled by orography. The region is characterized by frequent HPEs, and daily rainfall amounts

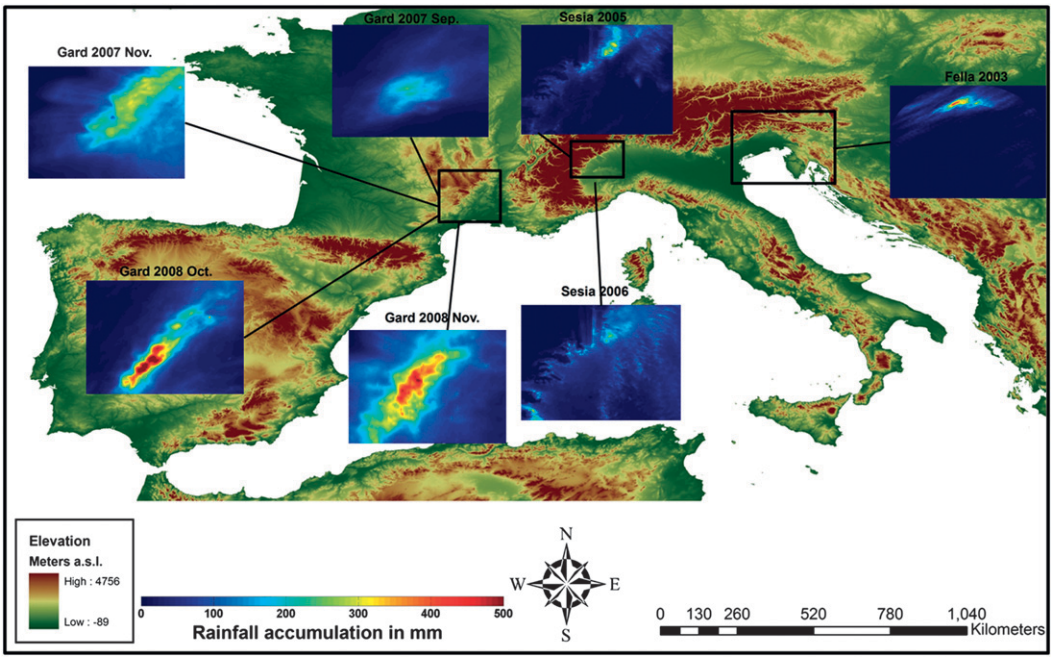

FIG. 1. Topography of central and southern Europe depicting the three selected study regions, marked with rectangular shapes, and the rainfall accumulation maps for each storm case.

exceeding 500 mm have been locally recorded in this area in a 20–30-yr time span (Borga et al. 2007). On 29 August 2003, after a prolonged drought, a mesoscale convective system affected the area, starting at 1000 local standard time (LST) and lasting for approximately 12 h (Borga et al. 2007). During the HPE, extremely high rain rates and rain accumulations were observed on the eastern tributaries of the Fella, whereas the west-side tributaries received much less rainfall (Borga et al. 2007). Overall, rainfall accumulation locally exceeded 350 mm, which is beyond doubt an extraordinary amount for a 12-h precipitation event. A striking characteristic of the event was its organization in four well-defined banded structures, some of which persisted in the same locations for the duration of the event (Borga et al. 2007), resulting in an astounding inhomogeneity of the rainfall accumulations throughout the region. The storm affected an area of 1500 km^2, causing losses of lives and immense problems in the local economy (Table 1).

Sesia is also located in northern Italy. More specifically, the Sesia River basin is a left-hand tributary of the Po River, with elevation ranging from 108 to 4555 m MSL (Sangati et al. 2009). The area is within the Piemonte region and is characterized by annual precipitation that ranges from 900 to 2000 mm, depending on elevation. Most of the basin's area is mountainous with steep slopes, and this topography is associated with the orographic enhancement of precipitation over the area. In general, the area is very frequently (once every two years), subject to calamitous storm events, especially on the upper part of the basin (Rabuffetti and Barbero 2005); two such events from this area are investigated in this study. The first storm was in early August 2005 (hereafter named Sesia 2005) and is characterized by two short convective storm episodes with duration of 6–8 h each occurring over the Sesia River basin (Sangati et al. 2009). The event lasted 18 h and its accumulated peak rainfall exceeded 220 mm, with hourly rainfall intensities up to 50 mm h^{-1}. The spatial extent of this storm was relatively small, but its overall impact was significant (Table 1). The second storm event (hereafter named Sesia 2006) took place on 15 September 2006 and lasted 23 h. It was characterized by mainly stratiform rainfall with small imbedded convective cells (Sangati et al. 2009), giving accumulated rainfall that reached 200 mm and rainfall rates up to 40 mm h^{-1} (Table 1).

The Cevennes–Vivarais is situated southeast of the Massif Central in France. The relief is a southeasterly facing slope starting from the Mediterranean shore and the Rhone valley (Younis et al. 2008). The elevation gradient is relatively weaker than the two northern Italy study areas (from sea level to 1700 m over roughly 70 km). The main Cevennes river basins are Virdourle, Ardeche, Ceze, and Gard and are characterized by a typical Mediterranean hydrological regime with very low levels of water in the summers and floods occurring

TABLE 1. General radar data characteristics.

Storm event	Start date	Duration (h)	Domain area (km^2)	Max. rainfall accumulation/rate (mm)/($mm\,h^{-1}$)	Avg rainfall rate ($mm\,h^{-1}$)	Coefficient of variation across time/space (dimensionless)	Correlation distance (km)	Rain fraction (%)	Fraction of rainfall rate $>10\,mm\,h^{-1}$ (%)	Fraction of rainfall rate $<1\,mm\,h^{-1}$ (%)
Fella 2003	29 Aug 0900 LST	12	81 600	329/65	1.28	1.61/3.33	16.40	18	11	48
Sesia 2005	2 Aug 0000 LST	18	23 552	222/48	1.32	1.55/2.45	14.75	27	4	53
Sesia 2006	15 Sep 0000 LST	23		181/40	2.04	1.31/2.37	53.24	41	2	33
Gard 2007 Sep	29 Sep 0600 LST	48	25 584	200/71	1.09	1.59/1.6	23.39	28	6	38
Gard 2007 Nov	19 Nov 0600 LST	96		286/24	1.26	1.21/1.15	65.99	45	2	34
Gard 2008 Oct	19 Oct 0600 LST	66		384/70	0.86	2.09/2.05	16.77	22	13	37
Gard 2008 Nov	31 Oct 0600 LST	48		434/59	2.85	1.0/1.0	32.27	74	7	22

mainly during fall (Younis et al. 2008). The four storm events selected for this study occurred in the Gard basin. The first event was on 29 September 2007 (hereafter named Gard 2007 Sep); its duration was 48 h, reaching a maximum accumulated rainfall of 200 mm. This storm was characterized by moderate average rainfall rate but included very high maximum rainfall intensities (up to $71\,mm\,h^{-1}$) (Table 1). The second event (hereafter named Gard 2007 Nov) was a relatively long-duration (96 h) event. Rainfall accumulations did not exceed 290 mm, while rainfall rates were up to $24\,mm\,h^{-1}$. This storm case was mainly stratiform-type precipitation (Table 1). The third event, (hereafter named Gard 2008 Oct) in October 2008 lasted 66 h, exhibiting high rainfall accumulations reaching a maximum of 400 mm over the Gard basin. Rainfall intensities were also high, with maximum intensities of $70\,mm\,h^{-1}$ (Table 1). The fourth event (Gard 2008 Nov) was a convective storm episode a few days later. It occurred in the period 31 October to 1 November 2008 and was characterized by extremely high rainfall accumulations (up to 440 mm) and high rainfall rates (up to $60\,mm\,h^{-1}$). The average rainfall rate for this storm was $2.85\,mm\,h^{-1}$ and its overall duration was 48 h (Table 1).

3. Data and methodology

The data used in this study are either radar-derived or satellite-retrieved rainfall. On the one hand, the radar data used for the Fella 2003 were derived from volume scan reflectivity data from a Doppler dual-polarized C-band Osservatorio Meteorologico Regionale (OSMER) radar station with a time resolution of 5 min and a spatial resolution of 250 m in range by 0.9° in azimuth. In this case, rainfall rates were estimated based on single-polarization reflectivity observations and differential reflectivity (ZDR) values were used to discriminate ground clutter from rainfall observations. On the other hand, the rainfall fields for the two Sesia storm cases (Sesia 2005 and Sesia 2006) were derived from volume scans of the Bric della Croce [L'Agenzia Regionale per la Protezione dell'Ambiente (ARPA), Piemonte, Italy] Doppler weather radar at a 1-km spatial resolution and 10-min time scale. Ten-minute rainfall data from 25 rain gauge stations in the Sesia River basin (with a spatial density of around 1 station per $100\,km^2$) were used to adjust radar rainfall estimates (Sangati et al. 2009). For all three storm events over Italy, several procedures were applied to the reflectivity observations in order to correct for the following error sources: 1) ground clutter, 2) partial beam occlusion, 3) path attenuation, and 4) wind drift. During the storm cases there was no observation of hail; hence, no correction was implemented

for hail contamination (Borga et al. 2007). The clutter-contaminated data in the polar volumes were flagged by an algorithm that used a three-step decision tree based on Doppler velocity, clear-air echo statistics, and ZDR variance (Bechini et al. 2002). Beam occlusion correction was based on offline computation of the percentage of beam power that was intercepted by the orography, using a model of beam propagation and a high-resolution (20 m) digital elevation model (Borga et al. 2000; Pellarin et al. 2002). For rain-path attenuation the correction was conducted using a variational method with gauge accumulations as external constraints and the Hitschfel-Bordan (1954) equation as attenuation correction model (Berenguer et al. 2002). The final radar rainfall estimates for the Fella, as well as for the two Sesia cases used in the analysis, involved a spatial resolution of 1000 m and a temporal aggregation of 30 min.

The radar rainfall estimation for the four Gard storm cases (2007 Sep, 2007 Nov, 2008 Oct, and 2008 Nov) was based on a careful analysis of the observation conditions for the radar systems available in the region (Bouilloud et al. 2010). First, a preprocessing step was aimed at checking the stability of the radar calibration by characterizing dry weather clutter and determining beam blockage for all elevation angles. Next, techniques for identifying clutter and rain types along with the corresponding vertical profiles of reflectivity (VPR) were implemented during the course of a rain event. Ground clutter was also used in checking the radar antenna positioning and geophysical errors by comparing observations and simulations based on the use of digital terrain models. VPR was either inferred from radar data if volume scanning data were available or simply defined with the 0°C isotherm altitude and the slope of the VPR above the 0°C isotherm. This information was then used in the correction of cluttered pixels through the refined interpolation techniques, and correction factor maps were plotted for each elevation angle to correct for range-dependent error sources (e.g., beam blockage). Finally, for the parameterization of the radar data processing, rather than applying a radar–rain gauge merging technique, an effective Z–R relationship was defined by comparing the radar and rain gauge rain amounts at the event time scale in the region hit by the rain event. This procedure was followed to ensure that the radar rainfall estimates are unbiased with respect to rain gauge rainfall at the event time scale. Radar rainfall estimates for the four Gard cases were hourly and available on a 1-km regular grid.

Two different high-resolution satellite rainfall products, CMORPH and PERSIANN, were assessed in this study; there are several differences between the two algorithms. The CMORPH technique produces global datasets of precipitation using exclusively passive microwave rainfall estimates derived from the low-orbit Special Sensor Microwave Imager (SSM/I), TRMM, Advanced Microwave Sounding Unit (AMSU), and Advanced Microwave Scanning Radiometer for Earth Observing System (EOS) (AMSR-E) satellites, whose features are propagated by motion vectors derived from geostationary satellite IR data (Joyce et al. 2004). The original product is created on a 0.07° grid at half-hourly temporal resolution, but 3-hourly 0.25° spatial resolution datasets are also available. For the purpose of this study, we chose the high-resolution (temporal and spatial) CMORPH data (0.07°/half-hourly), as we are dealing with short-term rainfall events that are characterized by localized, yet extreme, effects. All CMORPH data have a nearly global coverage and are available between 60°N and 60°S starting in December 2002.

PERSIANN is the other high-resolution, satellite-derived rainfall product utilized in this study. Hourly global Cloud Classification System (CCS) PERSIANN data, created on a 0.036° grid, are used to capture the extreme localized high-impact rainfall events. The PERSIANN CCS algorithm extracts local and regional cloud features from infrared (10.7 mm) geostationary satellite imagery, and using an automated neural network it estimates finer-scale rainfall distribution (Hong et al. 2007). The neural network parameters are regularly updated using TRMM Microwave Imager (TMI), SSM/I, and AMSU estimates (Hsu et al. 1997). PERSIANN CCS data cover the latitudinal range of 60°N to 60°S and start in 2002.

The error analysis in this paper was conducted at the nominal spatial resolution of CMORPH (0.07°), and all rainfall products (PERSIANN and radar) were therefore resampled at 0.07° grids and at hourly temporal scales. There are three categories of statistics used for this current analysis: 1) overall statistics that generally characterize the rainfall variability of each storm case, 2) performance statistics for the two selected satellite products, and 3) overall statistics for the two satellite products and for each storm event.

The various statistics used to characterize the storm events are shown in a tabulated form, and these are the coefficients of variation (standard deviation of the rain rates divided by the average rain rate) across time and space, rainfall correlation length, rain fraction, fraction of rainfall rates exceeding $10\,\mathrm{mm\,h^{-1}}$, and fraction of rainfall rates below $1\,\mathrm{mm\,h^{-1}}$. Correlation length characterizes the decay of the spatial correlation of the rainfall event studied, while the rain fraction defines the rain (spatial) coverage of the storm. The fraction of the rainfall rates that exceed $10\,\mathrm{mm\,h^{-1}}$ or are below $1\,\mathrm{mm\,h^{-1}}$ provide insight into the type of precipitation of the storm event (heavy versus light precipitation).

TABLE 2. Overall performance statistics of CMORPH and PERSIANN products for each storm event.

	Correlation coefficient (radar–CMORPH/radar-PERSIANN)	RMSE (mm) (radar–CMORPH/PERSIANN)	Bias ratio (radar–CMORPH/PERSIANN)
Storm event	Unconditional | Conditional	Unconditional | Conditional	Unconditional | Conditional
Fella 2003	0.63/0.49 | 0.61/0.65	3.84/5.09 | 8.28/11.98	0.96/0.44 | 0.54/0.28
Sesia 2005	0.54/0.53 | 0.69/0.80	3.33/3.67 | 4.95/7.39	0.60/0.21 | 0.73/0.42
Sesia 2006	0.51/0.47 | 0.44/0.38	3.30/3.62 | 4.64/5.63	0.64/0.29 | 0.60/0.38
Gard 2007 Sep	0.44/0.32 | 0.53/0.63	3.37/3.35 | 7.58/8.87	0.11/0.25 | 0.24/0.44
Gard 2007 Nov	0.64/0.30 | 0.53/0.35	1.71/2.20 | 3.29/3.74	0.28/0.40 | 0.47/0.50
Gard 2008 Oct	0.67/0.52 | 0.58/0.55	2.64/2.81 | 8.22/8.75	0.49/0.31 | 0.55/0.37
Gard 2008 Nov	0.51/0.38 | 0.53/0.42	4.17/4.27 | 6.67/6.17	0.19/0.28 | 0.32/0.47

The satellite retrieval performance metrics used in this study are shown as graphs plotted for various rainfall intensity bins and are the following: normalized mean error (NME), normalized random error standard deviation (NRESD), and normalized missed satellite rainfall volume (NMSRV). NME provides information about the differences between rainfall detected by the satellite products and the reference (radar), while NRESD is used to evaluate the variance of the estimation error. A point to note is that the random component of the satellite retrieval error does not account for the high systematic bias of the algorithm. It is therefore an estimate of the satellite's retrieval error variability. The NMSRV performance metric shows the radar rainfall volume that the satellite retrieval technique missed throughout the storm event, normalized by the total reference rainfall volume during that period. We calculated these metrics as follows:

$$\mathrm{NME} = \frac{\frac{1}{n}\sum[\mathrm{Sat}(c) - \mathrm{Rad}(c)]}{\frac{1}{n}\sum[\mathrm{Rad}(c)]}, \tag{1}$$

$$\mathrm{NRESD} = \frac{\mathrm{STDEV}\{[\mathrm{Sat}(c) \times \mathrm{Bias}(c)] - [\mathrm{Rad}(c)]\}}{\frac{1}{n}\sum[\mathrm{Rad}(c)]},$$

where

$$\mathrm{Bias} = \frac{\sum[\mathrm{Rad}(c)]}{\sum[\mathrm{Sat}(c)]}, \tag{2}$$

$$\mathrm{NMSRV} = \frac{\sum(\mathrm{Rad} > m \quad \text{and} \quad \mathrm{Sat} = 0)}{\sum(\mathrm{Rad} > 0)}. \tag{3}$$

Equations (1) and (2) are valid only for those pixels in time and space that satisfy criterion (c) according to which both satellite (Sat) and radar (Rad) indicate rain, but for different Rad rainfall intensity thresholds. Equation (3) is used for those pixels in time and space for which Sat indicates no rain but Rad does, and for various Rad thresholds (m). STDEV is standard deviation, while n is the number of events that satisfy a specific condition, which may change according to the rainfall regime or the investigated metric.

We also used overall error statistics, such as correlation coefficient (CC), root-mean-square error (RMSE), and bias ratio (BR), all presented in Table 2. The CC is calculated between the reference radar rainfall and each satellite product, while the RMSE is a quadratic measure of the magnitude of the difference between the sensor estimates and the reference rainfall. BR is defined as the ratio between the sensor's estimates to those of radar rainfall, and the closer it is to unity, the less biased the satellite estimates are. All statistics were calculated based on the radar domain of each storm event. The formulas for RMSE and BR are given below:

$$\mathrm{RMSE} = \sqrt{\frac{\sum(\mathrm{Sat} - \mathrm{Rad})^2}{n}}, \tag{4}$$

$$\mathrm{BR} = \frac{\sum(\mathrm{Sat})}{\sum(\mathrm{Rad})}. \tag{5}$$

Equations (4) and (5) are calculated for all pixels in space and time; the same is true for CC. RMSE, CC, and BR are metrics that were performed both unconditionally (including no-rain indicating pixels) and conditionally (for rain pixels only) for both satellite products and for each storm event.

4. Discussion of results

In an attempt to qualitatively assess the two satellite products investigated in this study, scatterplots for both

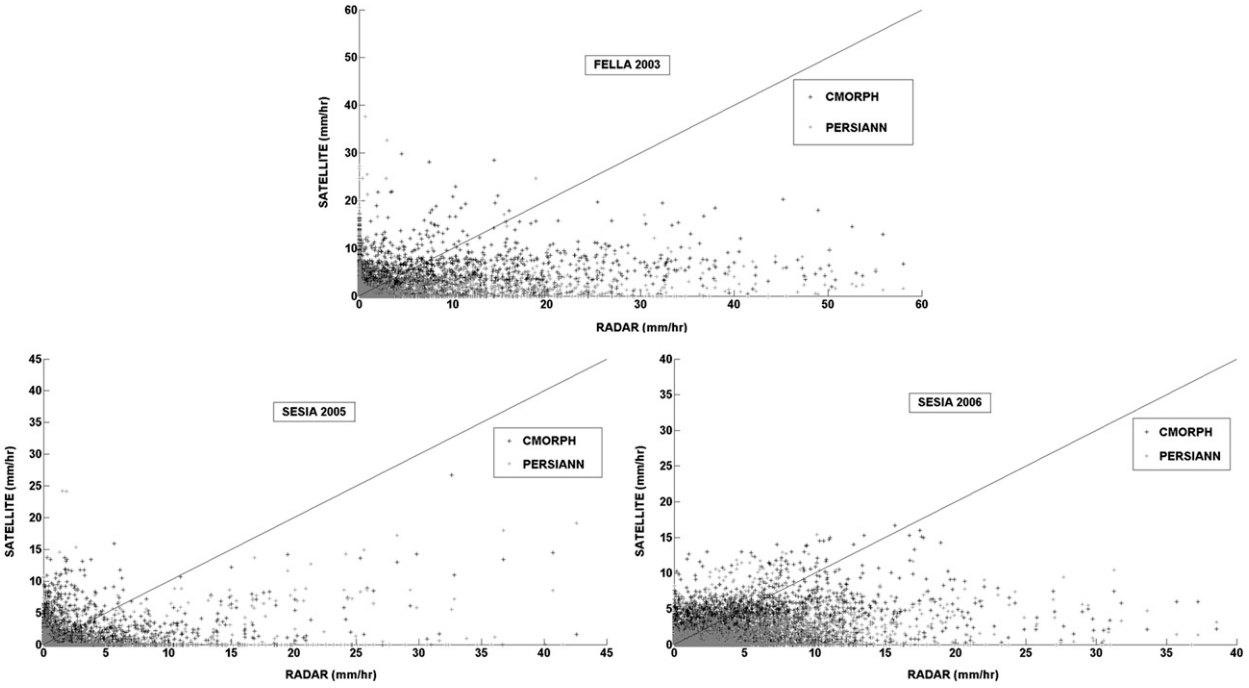

FIG. 2. Scatterplots of radar and satellite measurements for both CMORPH (dark gray) and PERSIANN (light gray) for the three storm events over northern Italy.

satellite techniques are shown in Figs. 2 and 3 for each storm event. Figure 2 shows the scatter diagrams for the three storm events that took place in northern Italy, while Fig. 3 shows those for the four storm cases of southern France. Evidently, in all storm events, the measurements of both satellite algorithms do not agree well with those of the radar, as they significantly underestimate the high rain rates and overestimate the light precipitation. In the following paragraphs, we quantitatively evaluate those differences using the error metrics discussed in section 3.

The NME exhibits positive values (overestimation) for low rainfall intensity for both CMORPH and PERSIANN and for all storm events studied (Fig. 4). However, as the rainfall intensity increases, NME values decrease, reaching a break point where NME becomes zero. This is true for both satellite techniques and for all storm cases, with the value of the aforementioned break point varying between the two satellite products and among the storm events. Beyond the break point, NME turns negative (underestimation), the absolute magnitude of which increases with increasing rainfall intensity. Remarkably, for both CMORPH and PERSIANN, all storm events exhibit similar NME values at very high rainfall rates, indicating severe underestimation (on the order of 60%–70%).

More specifically, there are two distinct patterns in CMORPH's NME (Fig. 4a): one that is followed by all three storm cases in Italy (Sesia 2005, Sesia 2006, and Fella 2003), as well as one in southern France (Gard 2008 Oct), and another pattern that is followed by the remaining three storm events in France (Gard 2007 Nov, Gard 2007 Sep, and Gard 2008 Nov). In the first cluster (Sesia 2005, Sesia 2006, Fella 2003, and Gard 2008 Oct), the NME varies significantly among the four storm events for very low rainfall intensity values (exhibiting high overestimation), but for moderate or high rainfall intensities, NME values agree well with each other among all four cases. NME becomes zero for these events at rain rates ranging from 2 to 4 mm hr^{-1}. In the other cluster, NME values are in good agreement with each other for all three storm events throughout all rainfall intensity bins, and the break point, where NME values change from positive to negative, takes place at rain rates around 1 mm h^{-1}. Notably, the overestimation of the three storm cases in Italy together with Gard 2008 Oct is substantially higher than that of the other storm events, at very low rain rates; this is attributed to the confounding effect of mixed rainfall areas, which are commonly found in most convective systems; typically, stratiform precipitation covers larger areas and contributes to a significant portion (40%–50%) of the rainfall volume of major convective systems (Anagnostou et al. 1999). Overall, the decay of NME values is much faster for the cases in Italy and the Gard 2008 Oct than the other three cases in France. The storm

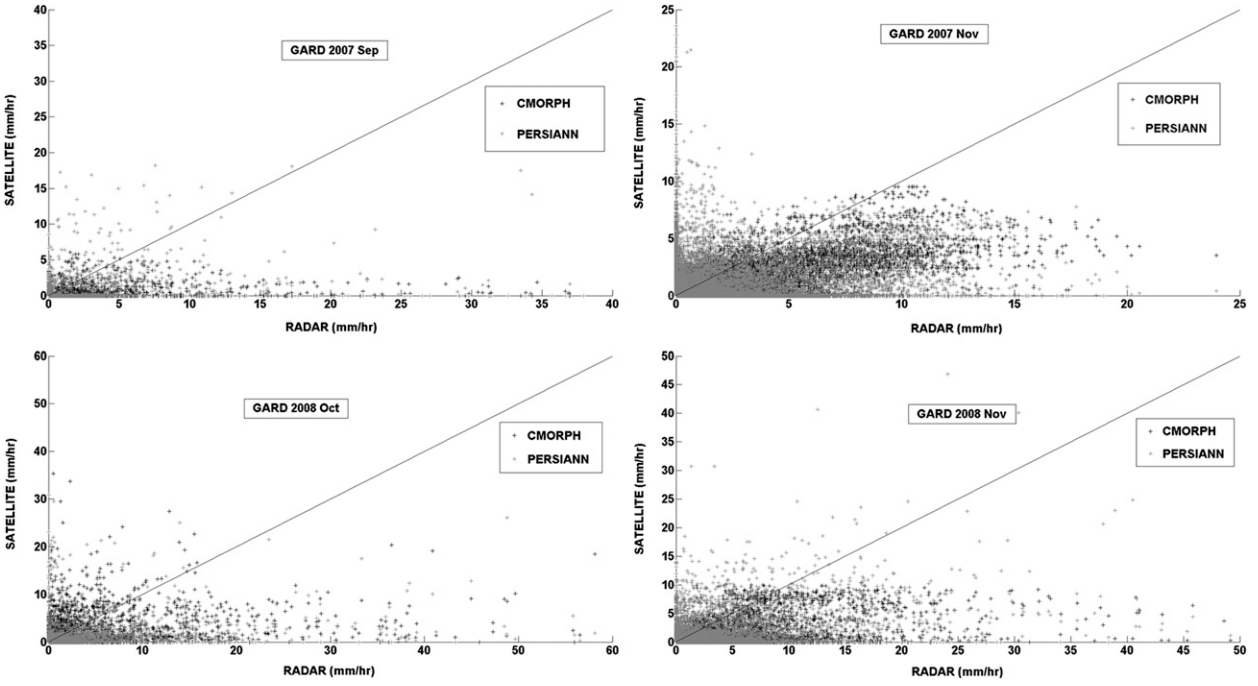

FIG. 3. Scatterplots of radar and satellite measurements for both CMORPH (dark gray) and PERSIANN (light gray) for the four storm events over southern France.

cases that exhibit relatively higher NME values for CMORPH (upper cluster in Fig. 4a) also have some common characteristics (Table 1); one such is that all three storm cases in northern Italy are characterized by the short duration of the event, whereas all of the other events have long durations. Moreover, all four events comprising the upper cluster in Fig. 4a have the highest coefficient of variation (CV) in space and are among the ones with the lowest rain fraction and correlation length (i.e., spatial correlation of rain rates). Finally, most of them exhibit a high fraction of rainfall rate exceeding $10\,\mathrm{mm\,hr^{-1}}$ (convective rainfall) and are among the ones with the highest maximum rainfall accumulations. The above characteristics of the storms reflect the differences between deep convective and more stratiform-dominated systems. Storm cases with low rain fraction, high convective fractional rainfall coverage, high maximum rainfall accumulations and CV in space, and low spatial correlation of rain rates clearly fall into the deep convective category; these storm cases are the ones that comprise the upper cluster in Fig. 4a. Storm events that are characterized by a high degree of spatial variation (high CV in space) will inevitably lead to higher retrieval errors.

PERSIANN, on the other hand, exhibits one common pattern for all storm cases (Fig. 4b). The break point where NME changes from positive to negative takes place

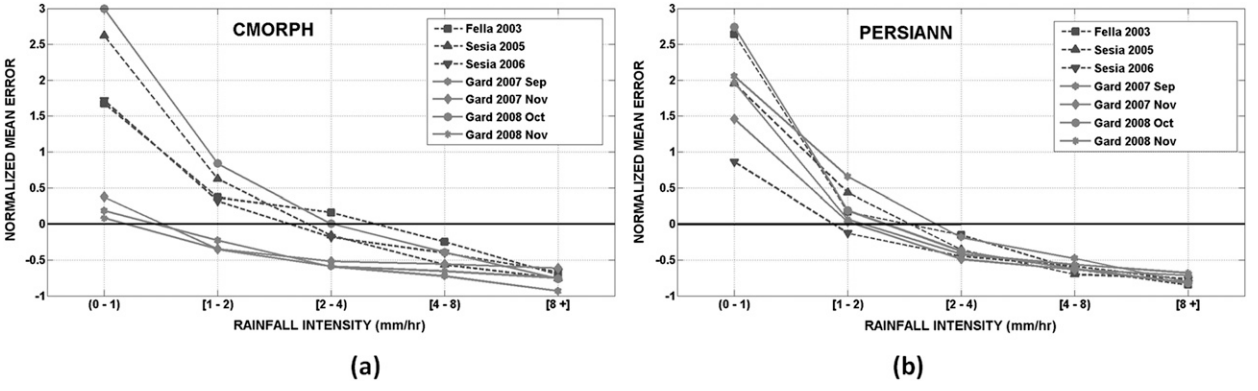

FIG. 4. NME for (a) CMORPH and (b) PERSIANN for different rainfall intensity thresholds.

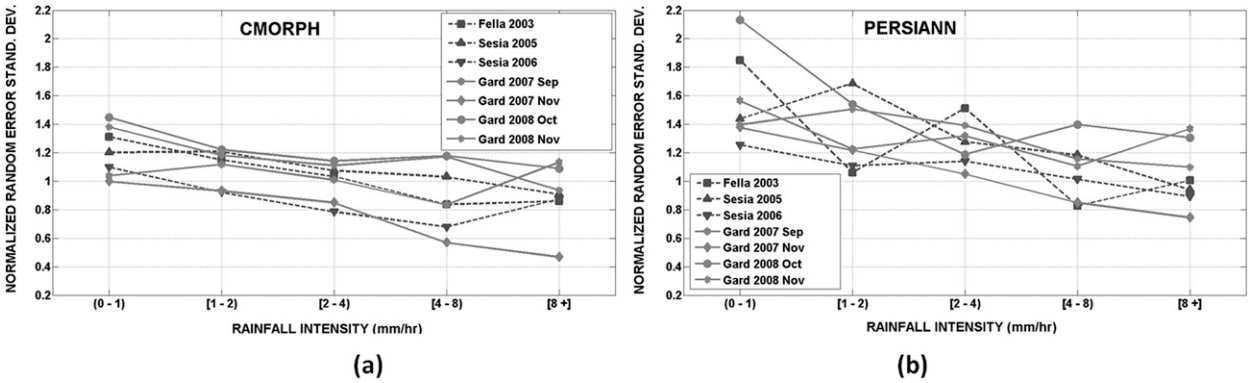

FIG. 5. NRESD for (a) CMORPH and (b) PERSIANN for different rainfall intensity thresholds.

at rain rates approximating 2 mm h^{-1}, and as rainfall intensity increases, NME values converge, indicating a strong underestimation of about 70%–80%. The decay of the NME values is similar among the various storm events, and as such, no distinct patterns between the deep convective storms and stratiform-type precipitation systems can be seen. Evidently, the IR imagery that is mainly used in the PERSIANN algorithm does not behave differently between the two aforementioned types of systems, potentially because of the lack of cloud penetration.

Both CMORPH and PERSIANN exhibit NRESD values that follow a decreasing trend with increasing rainfall intensity for all storm cases (Fig. 5); this is in agreement with the findings of AghaKouchak et al. (2012), who have shown that that systematic error of both retrievals increases as the rain rate increases. However, between the two algorithms, PERSIANN (Fig. 5b) exhibits higher NRESD values for most of the storm events and for all rainfall intensity bins. Furthermore, the NRESD values in the low rainfall intensity bins for PERSIANN are characterized by a broader range among the different storm events than for CMORPH (Fig. 5a). In general, NRESD values for CMORPH range from 0.5 to 1.4, whereas those for PERSIANN range from 0.8 to 2.1. NRESD for CMORPH shows more distinct patterns than for PERSIANN; regardless of the algorithm; however, two of the storm events show a constant behavior regarding NRESD. In both satellite techniques, Gard 2007 Nov and Sesia 2006 consistently exhibit the lowest NRESD values. These events are also characterized by the lowest fraction of rainfall rate exceeding 10 mm h^{-1}, the highest correlation length, and the lowest maximum rainfall rate and are among the storm cases with the highest rain fraction (Table 1). The aforementioned storm events are categorized as stratiform-dominated precipitation systems.

Another performance statistic used in this study is the fraction of the total rainfall volume that the satellite techniques fail to detect. We present this fraction as the NMSRV expressed as a percentage and plotted against various rainfall intensity categories (Fig. 6). As expected, by increasing the rainfall rate, the disagreement between satellite and radar rainfall detection tends to diminish because the satellite technique's rainfall detectability increases, and therefore, the NMSRV values decrease. In both satellite techniques, one can see that all three storm cases in Italy as well as the Gard 2008 Oct

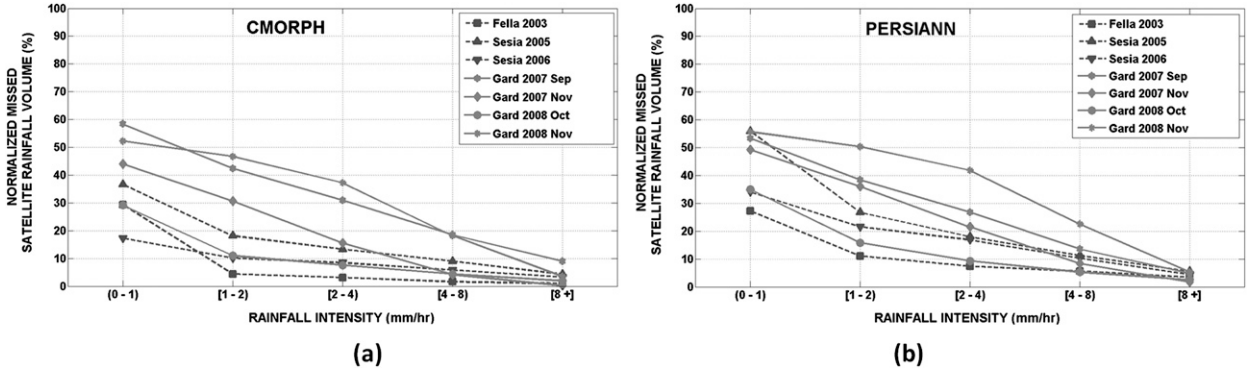

FIG. 6. NMSRV for (a) CMORPH and (b) PERSIANN for different rainfall intensity thresholds.

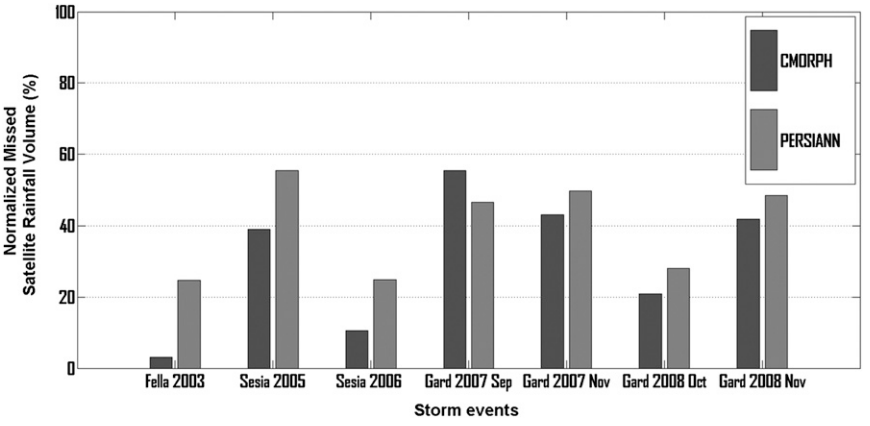

FIG. 7. Overall NMSRV for CMORPH and PERSIANN.

show a similar pattern of decay in their NMSRV values. The remaining three storm cases in France are characterized by patterns that are similar to each other. More specifically, Fella 2003, Sesia 2005, Sesia 2006, and Gard 2008 Oct exhibit lower NMSRV values for both satellite algorithms and for all rain rates, compared to Gard 2007 Sep, Gard 2007 Nov, and Gard 2008 Nov. The first group of storm events (lower NMSRV values) is composed of cases characterized by shorter duration, whereas the other three events lasted longer (Table 1). As noted in the NME analysis, all four events comprising the lower cluster in Figs. 6a and 6b have the highest CV in space and are among the ones with the lowest rain fraction and spatial correlation of rain rates. Finally, most of them exhibit a high fraction of rainfall rate exceeding $10\,\mathrm{mm\,h^{-1}}$ (heavy rainfall) are characterized by a moderate-to-high fractional coverage of rainfall rates that are smaller than $1\,\mathrm{mm\,h^{-1}}$, and are among the ones with the highest maximum rainfall accumulations (Table 1). Overall, as shown in Fig. 6, heavy rainfall episodes generated by deep convective systems, which are usually characterized by a high degree of spatial variation (low spatial correlation of rain rates and high coefficient of variation in space) and localized pockets of high rain rates resulting in high total accumulations, are more accurately detected by both CMORPH and PERSIANN algorithms, especially at high rain rates, while stratiform-type systems are less efficiently captured by the two algorithms, resulting in higher missed rainfall volumes compared to those associated with the deep convective storms. Although this is true for both rainfall algorithms, CMORPH was found to perform better than PERSIANN during most of the HPEs investigated in this study, and this is probably due to the fact that surface precipitation is more directly related to cloud properties inferred from MW than those inferred from IR.

In Fig. 7, we present the overall NMSRV in column bars for both satellite techniques. In six out of seven storm cases, PERSIANN misses rainfall to a greater extent than CMORPH, while in only one case in southern France (Gard 2007 Sep) CMORPH exhibits a higher NMSRV value than PERSIANN. Overall, PERSIANN is characterized by greater NMSRV values and in some storm events (Fella 2003, Sesia 2005, Sesia 2006) the difference in this metric between CMORPH and PERSIANN is significant. Among the different storm cases, Gard 2007 Sep, Gard 2007 Nov, Gard 2008 Nov, and Sesia 2005 exhibit the highest NMSRV values for both satellite techniques. This corroborates our hypothesis that these events include significant portions of light precipitation (rainfall rates below $1\,\mathrm{mm\,h^{-1}}$) that go undetected by passive microwave techniques.

In Table 2 we present overall statistics for both investigated satellite techniques and for each storm event separately. The conditional (i.e., for rainy pixels only) CC is consistently higher for CMORPH relative to PERSIANN (Table 2) when compared to the reference (radar). However, the unconditional CC is higher for CMORPH for four out of the seven events (Sesia 2006, Gard 2007 Nov, Gard 2008 Oct, and Gard 2008 Nov). Most of these events are characterized by the lowest CV in time, the highest rain fraction, the highest correlation length, and the lowest CV in space (Table 1).

The unconditional RMSE is higher for PERSIANN for all events but the Gard 2007 Sep (Table 2), which is characterized by relatively low maximum rainfall accumulation and average rain rates. Similarly, the conditional RMSE is higher for PERSIANN for all storm events except for the case of Gard 2008 Nov, which is characterized by the highest maximum rainfall accumulation, highest average rainfall rate, the lowest CV in time and space, and the highest rain fraction (Table 1).

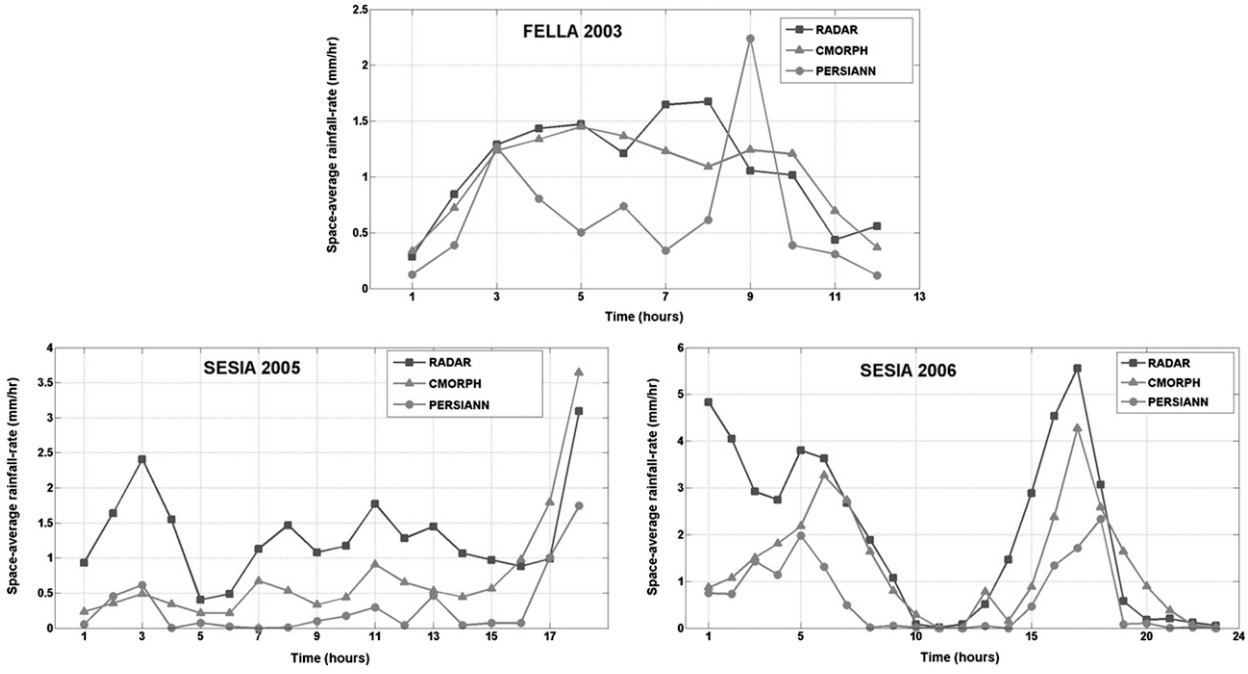

FIG. 8. Time series of domain-averaged rainfall rate for radar, CMORPH, and PERSIANN for the three storm events over northern Italy. The scales on the *x* and *y* axes are not the same among the three cases.

The BR (conditional or unconditional) is always lower than 1, indicating rainfall underestimation for all storm cases and both satellite techniques (Table 2). These findings agree with those of Demaria et al. (2011), who showed that satellite estimates of high rainfall rates from both CMORPH and PERSIANN were at all times lower than observed values, as well as those of Turk et al. (2006), who found that CMORPH underestimated heavy rainfall both over land and ocean. More specifically, BR is closer to unity (less underestimation) for CMORPH than for PERSIANN for the Sesia 2005, Sesia 2006, Fella 2003, and Gard 2008 Oct events. These events exhibit a relatively higher NME for CMORPH, especially for low rainfall intensity values (Fig. 4), and are characterized by high CV values in time and space, low rain fraction and low correlation lengths (Table 1). Moreover, the same storm cases are characterized by lower NMSRV values for both satellite algorithms and for all rain rates (Fig. 6). For all the other storm events CMORPH BR is lower (more underestimation) than the PERSIANN BR.

Finally, we present the time series of the domain-averaged rainfall rate for CMORPH, PERSIANN, and radar for all the storm cases examined in this study (Figs. 8, 9). Figure 8 shows the time series for the storm cases over Italy, whereas Fig. 9 shows the storm cases over France. In the case of the two Sesia (2005 and 2006) events (Fig. 8), it is evident that both satellite algorithms underestimate rainfall at all times, with PERSIANN exhibiting the highest underestimation. However, despite their quantitative differences with respect to the reference (radar), both CMORPH and PERSIANN perform well in terms of capturing the event (especially in the case of Sesia 2006). Fella 2003, on the other hand, shows a general agreement between CMORPH and radar and an underestimation from PERSIANN, with an instant overestimation toward the end of the event and without capturing well the event. As far as the four cases in France (Fig. 9), we note an overall underestimating trend for both satellite techniques, but with a few incidents of overestimation. The temporal evolution of the storm events is not well captured in the cases of Gard 2007 Sep, Gard 2007 Nov, and Gard 2008 Nov; the heavy-rainfall parts of the storms, however, are sufficiently represented in both satellite rainfall products. Gard 2008 Oct is the only storm case in France where the two satellite techniques captured the event well (especially the part of the event characterized by high rain rates).

5. Conclusions

We can draw several conclusions from the findings of this study. For most of the storm events, CMORPH is characterized by higher CCs, lower missed rainfall volumes, and better bias ratios than PERSIANN. Thus, its

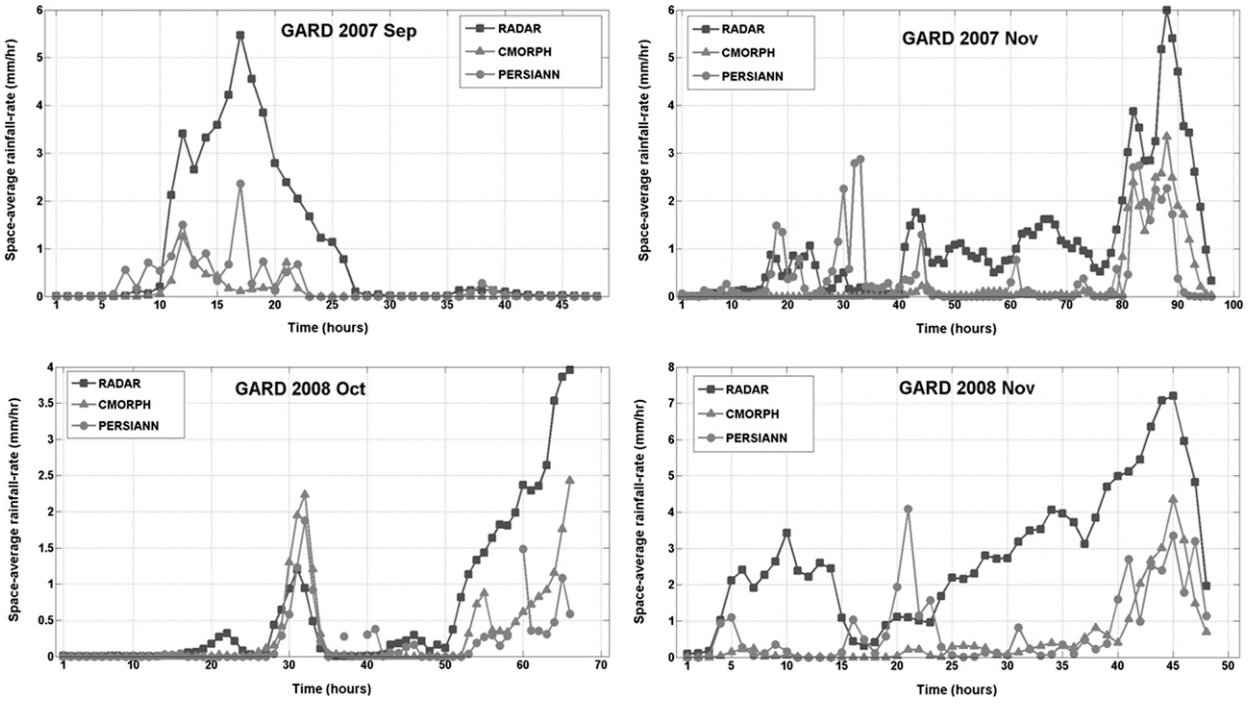

FIG. 9. As in Fig. 8, but for the four storm events over southern France.

performance in regards to the heavy precipitation events examined in this study can be deemed better than that of PERSIANN. In terms of NME, the type of precipitation plays an important role in determining the magnitude of CMORPH's error, but only for low-to-medium rainfall rates, where deep convective precipitation events are characterized by higher error than stratiform-dominated rainfall systems, while for high rainfall intensity values, the type of precipitation does not seem to influence the magnitude of the error, as both convective and stratiform-dominated types of precipitation exhibit almost identical errors. In the case of PERSIANN there is no clear relationship between precipitation type and error characteristics.

Both satellite techniques underestimated rainfall for all storm cases, at all times, and especially at high rainfall rates. PERSIANN was found to underestimate to a greater extent than CMORPH. The PERSIANN's tendency to underestimate more than CMORPH can be attributed to the fact that IR measurements are not adequately physically related to precipitation. Differences in the magnitude of underestimation can be associated to the type of precipitation. Within each event, and for very low rainfall rates, rainfall is always overestimated by both satellite techniques. The underestimation of all the other rainfall regimes (especially at high rain rates), however, is much greater in magnitude. Overall, the higher errors associated with the convective storm cases could be attributed to the fact that most of these events are characterized by mixed rainfall areas and a high degree of spatial variability, thus leading to greater retrieval errors.

The NRESD of CMORPH was found to be generally lower than that of PERSIANN, regardless of the storm event, or the rainfall regime, while the missed rainfall volume by PERSIANN was for most of the investigated cases larger than that for CMORPH, and it was greater for the stratiform-dominated storm cases. The type of retrieval technique determines the restrictions and capabilities of the precipitation estimation. More specifically, the ability of CMORPH to provide information about the entire cloud profile, while PERSIANN does not, is probably the reason for the differences in the missed rainfall volume between the two algorithms.

Fella 2003, Sesia 2005, and Sesia 2006 (and Gard 2008 Oct, to a lesser extent) are characterized by bias ratio values that are closer to unity (especially for CMORPH) and higher RMSE values (especially for PERSIANN). Taking into account the deep convective type of precipitation associated with those storm cases, we can conclude that the morphing procedure (CMORPH) captures convective events better than the adaptive neural network calibration of IR imagery (PERSIANN). Differences in the type of precipitation (convective versus stratiform) therefore have an effect on the algorithm's ability to capture rainfall effectively. Geographical factors also determine the performance of the satellite. In our

results, clustering of events that are characterized by geographical proximity indicates that satellite techniques perform in a certain ''fashion'' over a specific region, probably because of topographic and climatic similarities, which undoubtedly affect the retrieval's ability.

The results of this study are valid for heavy convective or mixed-phase precipitation events occurring over the aforementioned mountainous regions. Although we cannot extend the validity of the present findings to other hydroclimatic regimes, or draw generalized conclusions, the results of this study clearly show that despite the relentless improvement in the accuracy and robustness of satellite-based precipitation estimation algorithms, many challenges still remain in the development of these algorithms, especially for heavy/extreme precipitation events. This analysis offers important knowledge about the deficiencies of two of the major satellite-based rainfall retrieval algorithms when it comes to flood-inducing heavy rain rates over complex terrain, and its findings indicate the existence of different behavioral patterns of the satellite techniques investigated (depending on the event severity and duration, the topography of the area and precipitation type, etc.). Our main premise is that more analyses and investigations over different geographical regions and climatic regimes, and for a more extensive record of HPEs, will shed light on this challenge facing satellite rainfall-retrieval algorithms, and more clear patterns in the satellite techniques' behavior will emerge. Future continuation of this work would include investigating the error of the same and other satellite retrieval techniques over other geographical regions of the world and for storm cases of different intensities and duration. Furthermore, the present analysis will be used as the basis for developing a satellite error model for ensemble representation of satellite rainfall and satellite-driven flood modeling over complex terrain basins.

Acknowledgments. This work was supported by a NASA Precipitation Measurement Mission award (NNX07AE31G). We also acknowledge and appreciate Prof. Marco Borga of the University of Padua and Prof. Guy Delrieu of the Laboratoire d'Etude des Transferts en Hydrologie et Environnement (LTHE) for providing the radar rainfall data for the flood cases in the Italian and French basins, respectively.

REFERENCES

Adler, R. F., G. J. Huffman, D. T. Bolvin, S. Curtis, E. J. Nelkin, 2000: Tropical rainfall distributions determined using TRMM combined with other satellite and rain gauge information. *J. Appl. Meteor.,* **39,** 2007–2023.

AghaKouchak, A., A. Behrangi, S. Sorooshian, K. Hsu, and E. Amitai, 2011: Evaluation of satellite-retrieved extreme precipitation rates across the central United States. *J. Geophys. Res.,* **116,** DO2115, doi:10.1029/2010JD014741.

——, A. Mehran, H. Norouzi, and A. Behrangi, 2012: Systematic and random error components in satellite precipitation data sets. *Geophys. Res. Lett.,* **39,** L09406, doi:10.1029/2012GL051592.

Anagnostou, E. N., A. J. Negri, and R. F. Adler, 1999: A satellite infrared technique for diurnal rainfall variability studies. *J. Geophys. Res.,* **104** (D24), 31 477–31 488.

——, V. Maggioni, E. I. Nikolopoulos, T. Meskele, F. Hossain, and A. Papadopoulos, 2010: Benchmarking high-resolution global satellite rainfall products to radar and rain-gauge rainfall estimates. *IEEE Trans. Geosci. Remote Sens.,* **48,** 1667–1683.

Artan, G., H. Gadain, J. L. Smith, K. Asante, C. J. Bandaragoda, and J. P. Verdin, 2007: Adequacy of satellite derived rainfall data for stream flow modeling. *Nat. Hazards,* **43,** 167–185.

Bechini, R., E. Gorgucci, G. Scarchilli, and S. Dietrich, 2002: The operational weather radar of Fossalon di Grado (Gorizia, Italy): Accuracy of reflectivity and differential reflectivity measurements. *Meteor. Atmos. Phys.,* **79,** 275–284.

Berenguer, M., G. W. Lee, D. Sempere-Torres, and I. Zawadzki, 2002: A variational method for attenuation correction of radar signal. *Proc. Second European Conf. on Radar Meteorology,* Delft, Netherlands, Delft University of Technology, 11–16.

Borga, M., E. N. Anagnostou, and E. Frank, 2000: On the use of real-time radar rainfall estimates for flood prediction in mountains basins. *J. Geophys. Res.,* **105** (D2), 2269–2280.

——, P. Boscolo, F. Zanon, and M. Sangati, 2007: Hydrometeorological analysis of the 29 August 2003 flash flood in the eastern Italian Alps. *J. Hydrometeor.,* **8,** 1049–1067.

Bouilloud, L., G. Delrieu, B. Boudevillain, and P. E. Kirstetter, 2010: Radar rainfall estimation in the context of post-event analysis of flash-floods. *J. Hydrol.,* **394,** 17–27.

Demaria, E. M. C., D. A. Rodriguez, E. E. Ebert, P. Salio, F. Su, and J. B. Valdes, 2011: Evaluation of mesoscale convective systems in South America using multiple satellite products and an object-based approach. *J. Geophys. Res.,* **116,** D08103, doi:10.1029/2010JD015157.

Dinku, T., S. Chidzambwa, P. Ceccato, S. J. Connor, and C. F. Ropelewski, 2008: Validation of satellite rainfall products over East Africa's complex topography. *Int. J. Remote Sens.,* **29,** 4097–4110.

Ducrocq, V., O. Nuissier, D. Ricard, C. Lebeaupin, and T. Thouvenin, 2008: A numerical study of three catastrophic precipitating events over southern France. II: Mesoscale triggering and stationarity factors. *Quart. J. Roy. Meteor. Soc.,* **134,** 131–145.

Gaume, E., and Coauthors, 2009: A compilation of data on European flash floods. *J. Hydrol.,* **367,** 70–78.

Groisman, P. Ya, R. W. Knight, T. R. Karl, D. R. Easterling, B. Sun, and J. Lawrimore, 2004: Contemporary changes of the hydrological cycle over the contiguous United States: Trends. *J. Hydrometeor.,* **5,** 64–85.

——, ——, ——, ——, G. C. Hegerl, and V. N. Razuvaev, 2005: Trends in intense precipitation in the climate record. *J. Climate,* **18,** 1326–1350.

Gruber, A. V., and V. Levizzani, 2006: Assessment of global precipitation products: A project of the World Climate Research Programme Global Energy and Water Cycle Experiment (GEWEX) Radiation Panel. WCRP-128/WMO/TD-1430, 50 pp. [Available online at http://www.gewex.org/reports/2008AssessmentGlobalPrecipReport.pdf.]

Hitschfeld, W. F., and J. Bordan, 1954: Errors inherent in the radar measurement of rainfall at attenuating wavelengths. *J. Meteor.,* **11,** 58–67.

Hong, Y., D. Gochis, J. T. Cheng, K. L. Hsu, and S. Sorooshian, 2007: Evaluation of PERSIANN-CCS rainfall measurement using the NAME Event Rain Gauge Network. *J. Hydrometeor.,* **8,** 469–482.

Hsu, K., X. Gao, S. Sorroshian, and H. Gupta, 1997: Precipitation estimation from remotely sensed information using artificial neural networks. *J. Appl. Meteor.,* **36,** 1176–1190.

Huffman, G. J., R. F. Adler, D. T. Bolvin, G. Gu, E. J. Nelkin, K. P. Bowman, Y. Hong, E. F. Stocker, and D. B. Wolff, 2007: The TRMM multi-satellite precipitation analysis: Quasi-global, multi-year, combined-sensor precipitation estimates at fine scale. *J. Hydrometeor.,* **8,** 38–55.

Jiang, H., J. B. Halverson, and E. J. Zipser, 2008: Influence of environmental moisture on TRMM-derived tropical cyclone precipitation over land and ocean. *Geophys. Res. Lett.,* **35,** L17806, doi:10.1029/2008GL034658.

Joyce, J. R., E. J. Janowiak, P. A. Arkin, and P. Xie, 2004: CMORPH: A method that produces global precipitation estimates from passive microwave and infrared data at high spatial and temporal resolution. *J. Hydrometeor.,* **5,** 487–503.

Kidd, C., R. D. Kniveton, C. M. Todd, and J. T. Bellerby, 2003: Satellite rainfall estimation using combined passive microwave and infrared algorithms. *J. Hydrometeor.,* **4,** 1088–1104.

Krajewski, W. F., and J. A. Smith, 2002: Radar hydrology-rainfall estimation. *Adv. Water Resour.,* **25,** 1387–1394.

Levizzani, V., 1999: Convective rain from a satellite perspective: Achievements and challenges. *SAF Training Workshop: Nowcasting and Very Short Range Forecasting,* EUMETSAT, 75–84.

Maddox, R., J. Zhang, J. J. Gourley, and K. W. Howard, 2002: Weather radar coverage over the contiguous United States. *Wea. Forecasting,* **17,** 927–934.

Michaelides, S., V. Levizzani, E. Anagnostou, P. Bauer, T. Ksparis, and J. E. Lane, 2009: Precipitation: Measurement, remote sensing, climatology and modeling. *Atmos. Res.,* **94,** 512–533.

Pellarin, T., G. Delrieu, M. Saulnier, H. Andrieu, B. Vignal, and J. D. Creutin, 2002: Hydrologic visibility of weather radar systems operating in mountainous regions: Case study for the Ardeche catchment (France). *J. Hydrometeor.,* **3,** 539–555.

Prat, O. P., and A. P. Barros, 2010: Assessing satellite-based precipitation estimates in the Southern Appalachian Mountains using rain gauges and TRMM PR. *Adv. Geosci.,* **25,** 143–153.

Rabuffetti, D., and S. Barbero, 2005: Operational hydrometeorological warning and real-time flood forecasting: The Piemonte Region case study. *Hydrol. Earth Syst. Sci.,* **9,** 457–466.

Salio, P., Y. G. Skabar, and M. Nicolini, 2007: Flash flood event over central Argentina: A case study. Preprints, *Fourth European Conference on Severe Storms,* Trieste, Italy, Abdus Salam International Centre for Theoretical Physics, 10 pp. [Available online at ftp://ftp.cima.fcen.uba.ar/pub/yanina/salio_skabar_nicolini.pdf.]

Sangati, M., M. Borga, D. Rabuffetti, and R. Bechini, 2009: Influence of rainfall and soil properties spatial aggregation on extreme flash flood response modeling: An evaluation based on the Sesia river basin, north western Italy. *Adv. Water Resour.,* **32,** 1090–1106.

Sapiano, M. R. P., and P. A. Arkin, 2009: An intercomparison and validation of high-resolution satellite precipitation estimates with 3-hourly gauge data. *J. Hydrometeor.,* **10,** 149–166.

Scheel, M. L. M., M. Rohrer, C. Huggel, D. Santos Villar, E. Silvestre, and G. J. Huffman, 2010: Evaluation of TRMM Multi-satellite Precipitation Analysis (TMPA) performance in the Central Andes region and its dependency on spatial and temporal resolution. *Hydrol. Earth Syst. Sci. Discuss.,* **7,** 8545–8586.

Schumacher, C., and R. A. Houze Jr., 2003: The TRMM precipitation radar's view of shallow, isolated rain. *J. Appl. Meteor.,* **42,** 1519–1524.

Scofield, R. A., and R. J. Kuligowski, 2003: Status and outlook of operational satellite precipitation algorithms for extreme-precipitation events. *Wea. Forecasting,* **18,** 1037–1051.

Stampoulis, D., and E. N. Anagnostou, 2012: Evaluation of global satellite rainfall products over continental Europe. *J. Hydrometeor.,* **13,** 588–603.

Steiner, M., and J. A. Smith, 1998: Convective versus stratiform rainfall: An ice-microphysical and kinematic conceptual model. *Atmos. Res.,* **47–48,** 317–326.

Tang, L., and F. Hossain, 2012: Investigating the similarity of satellite rainfall error metrics as a function of Koppen climate classification. *Atmos. Res.,* **104–105,** 182–192.

Turk, F. J., G. J. Huffman, R. Joyce, C. Kidd, and R. Kuligowski, 2006: Evaluation of satellite-based estimates of precipitation in the Yucatan region during Hurricane Wilma. Preprints, 27th Conf. on Hurricanes and Tropical Meteorology, Monterey, CA, Amer. Meteor. Soc., P1.5. [Available online at https://ams.confex.com/ams/pdfpapers/108948.pdf.]

Younis, J., S. Anquetin, and J. Thielen, 2008: The benefit of high-resolution operational weather forecasts for flash flood warning. *Hydrol. Earth Syst. Sci. Discuss.,* **5,** 345–377.